Theory and application of the Mean Exponential Growth of Nearby Orbits (MEGNO)

Qiulin Li

May 2023

Abstract

The study of Chaos in Dynamical systems has risen in popularity in recent decades. Increased interest in chaos dynamics has resulted in many advancements in the field as well as the emergence of new Chaos indicators. The maximum Lyapunov Characteristic Exponent (mLCE) is one of the oldest and most important chaos indicator used in chaos theory, however, there are several new chaos indicators based off of the mLCE that have been shown to detect chaos better. This report will present MEGNO (Mean Exponential Growth of Nearby Orbits), a new chaos indicator based off of the mLCE that can detect chaos more efficiently. This paper will also provide a brief overview on topics needed to understand MEGNO, including a brief discription of the mLCE itself.

Contents

1 Introduction

Many phenomena that appear random and irregular are often grounded in systems with structure (Wigmore, 2016). The idea behind chaos is that small changes in the inital conditions of a system can result in wildly random or stochastic behaviour. There have been many attempts to describe the random nature of these phenomena, with the most successful explanation coming from Chaos Theory, a subfield of Dynamical systems(Wells, 2022).

The study of Dynamical systems has largely been concerned with discovering, quantifying and predicting chaos since its' discovery in 1963 by Lorentz (Strogatz & Dichter, 2016). Since then, Chaos theory has developed immensely and along with it, tools to detect and identify chaos. These tools, also known as chaos indicators, can be used to identify the presence and prevalance of chaos in a system. One of the first chaos indicators, known as the maximum Lyapunov Characteristic Exponent (mLCE) has been widely used to detect chaos in many dynamical systems (Skokos, 2010). This report will introduce a modern chaos indicator known as the MEGNO indicator that has been shown to be a better alternative to the mLCE (Cincotta & Giordano, 2016).

2 Chaos Theory

Trajectories flow in various ways in a dynamical system. These Trajectories often take on the form of orbits thar can be periodic and quasiperiodic. Periodic orbits will occur at regular intervals, whereas quasi-periodic orbits occur at irregular and somewhat random intervals. Both periodic and quasiperiodic trajectories behave in a mannner that is considered Regular. Non-regular trajectories are known as Chaotic trajectories that flow randomly. There have been many attempts to define Chaos, we will begin with its' general definition according to Strogatz & Dichter (2016).

"Chaos is aperiodic long-term behavior in a deterministic system that exhibits sensitive dependence on initial conditions."

This definition provides a broad overview of chaotic behaviour, however it provides no criteria to determine exactly whether a trajectory is chaotic. Devaney (2021) developed a definition of chaos that also provides a criteria for a trajectory to be chaotic. If f is a mapping defined as $f : V \to V$ where V is the Phase Space of the system, we can say f is chaotic if:

1. f has a sensitive dependence on initial conditions. Trajectories that start near each other seperate quickly (Strogatz & Dichter, 2016)
2. f is topologically transitive. Points that start in one neighbourhood will move iteratively into different regions.
3. Periodic points are dense in V. These points imply an underlying structure that exists in all chaotic systems. (Devaney, 2021)

If a system has a mapping f can satisfy all three of Devaney's conditions, it is considered chaotic. Regular trajectories in an autonomous Hamiltonian system produces orbits bound on an invariant tori. If chaotic orbits emerge, the trajectories are no longer bound by a tori and cantori typically emerge(Dvorak, 1999). Orbits are often difficult to visualise in position space (x, y) due to their swirling behaviour, however a shift to Phase space (x, px), also known as position-momentum space, will allow us to use Poincare surface sections to visualise these flows better.

2.1 Visualising Chaos: Poincare Sections

Poincaré surface sections (PSS) are often used to visualise swirling flows in a dynamic system (Strogatz & Dichter, 2016). The Surface section plots are produced by mapping N-dimensional continuous flow into 2

dimensional Discrete points that are then plotted in Phase space. The surface section is a plane that is perpendicular to the trajectory of a particle in a system. According to(Strogatz & Dichter, 2016), Poincare Surface sections are defined as:

The Poincaré map P is a mapping from S to itself, obtained by following trajectories from one intersection with S to the next. If $x_k \in S$ denotes the kth intersection, then the Poincaré map is defined by

$$x_{k+1} = P(x_k)$$

We can approximate solutions to any mapping using numerical methods. A particularly good method is described by Henon in (Henon, 1982) that can be used to produce extremely accurate approximations of points on a PSS section. An autonomous system with 2 degrees of freedom in four dimensional phase space shown in Figure 1, along with the Poincaré map that is the 2D surface that is perpendicular to the swirl of flow.

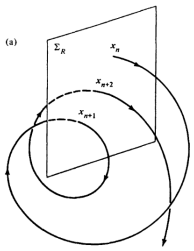

Figure 1: Poincaré surface and its' computation

Poincaré maps can often indicate whether a system is periodic or chaotic (Strogatz & Dichter, 2016)], however this is not always the case. This is especially true when sticky orbits are visualised.

2.2 Sticky Orbits

Sticky orbits are trajectories that spend a long time near stable regions but will eventually escape to chaotic regions(Dvorak, 1999). There are two different types of sticky orbits as described by Contopoulous (2008). The first type is stickiness around islands of stability, which will be the primary sticky orbits we find in these papers. The second type is sticky orbits that occur along the unstable asymptotic curve of quasiperiodic orbits. In this report we will focus on the first type of stickiness that appears around islands of stability. These regions where stickiness occurs are often characterised by cantori. The cantori are remnants of the torus that is destroyed when chaos emerges (Dvorak,1999).

Sticky orbits exhibit a special type of chaotic behaviour since it will satisfy all the criterion for chaos after a long enough time period(Contopoulous, 2008). The presence of these sticky orbits makes it difficult to differentiate between chaotic and regular orbits. Seemingly regular orbits can actually be sticky after sufficiently long time periods and even then, it is difficult to differentiate between sticky and regular orbits visually. Chaos indicators are often used to classify chaos, sticky and regular trajectories. The computation of these chaos indicators often require a method of quantifying how nearby trajectories of a system behave relative to one another.

3 Dynamic Systems, Variational Equations and Tangent Maps

A trajectory in an N-dimensional Hamiltonain system can be written as $x_i(\tau) = (x_1, x_2 ... x_N)$. In order to determine whether the behaviour of trajectories we must evolve the initial trajectory x_i as well as some nearby trajectory x_n and see how they evolve relative to one another. The distance between x_i and x_n is known as the deviation vector $\overrightarrow{v}$, that varies over time (Benettin & Galgani, 1979). The nearby trajectory as well as the deviation vector at time t are shown in equation 1 and 2.

$$x_n(t) = (x_1 + \delta 1, x_2 + \delta 2 ... x_n + \delta n) \tag{1}$$

$$\overrightarrow{v} = (\delta x_1, \delta x_2, ... \delta x_n)^t \tag{2}$$

The Euclidian norm (magnitude) of the Deviation vector $\overrightarrow{v}$ can grow and shrink over over time. This is illustrated in figure 2 where v increases as time progresses.

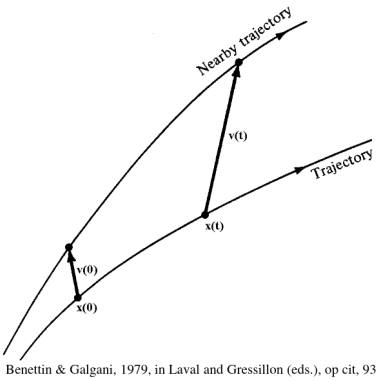

Benettin & Galgani, 1979, in Laval and Gressillon (eds.), op cit, 93

Figure 2: Deviation Vector, (Benettin & Galgani, 1979, in Laval and Gressillon (eds.), op cit, 93)

The trajectories of a system evolve in position space via equations of motion. The vector $\overrightarrow{v}$, will change in position space over time, however, this requires the computation of the original trajectory, the neighbouring trajectory as well as the $\overrightarrow{v}$ itself. The computation of the deviation vector $\overrightarrow{v}$ can be simplified if we evolve it in the Tangent space instead.
In the Tangent Space, the deviation vector evolves via some linear mapping (Skokos, 2010) that will evolve $\overrightarrow{v}(t)$ to $\overrightarrow{v}(t+1)$ by iterating it over some mapping. Variational equations are the mappings will allow us to time evolve the Deviation vector in tangent space. Evolving v using variational equations has the added bonus of being easier to compute, since it does not require the evolution of a nearby trajectory. There are several ways to derive the variational equations of a system. These methods differ based on whether the system is continuous or discrete.

3.1 Continuous Systems and the Tangent method

The Tangent Method is used to find the Variational Equations of Continuous Dynamical Systems. Continuous dynamical systems are generally given in the form

$$\dot{x} = \frac{dx}{dt} = f(x,t) \tag{3}$$

where f denotes a series of vector fields(Skokos, 2010). Hamiltonian systems are usually continuous and hence are written in the form shown above. The solution to these systems, also known as flows, can behave in a variety of ways, the flows can be regular, periodic, quasiperiodic or chaotic (Strogatz & Dichter, 2016). The Tangent method requires that the dynamical system must firstly be rewritten in matrix form. The formula that is used to produce the variational equations is written concisely in equation 4 (Skokos, 2010) with **J, P** representing $2N \times 2N$ matrices where N is the dimensions of the system.

$$\dot{V} = \frac{dv}{dt} = -J \cdot P \cdot \overrightarrow{v} \tag{4}$$

The Elements of Matrix **P** is shown in equation 5) where i is the row number and j denotes the column number of each element of the matrix.

$$P_{i,j} = \frac{\partial H}{\partial x_i \partial x_j} \tag{5}$$

J denotes the Jacobian of the system. Given some discrete system in the form of equation 7, the Jacobian can be written as shown in equation 6 according to Skokos (2010).

$$J = \frac{\partial \mathbf{f}}{\partial \mathbf{x}} = \begin{bmatrix} \frac{\partial f_1}{\partial x_1} & \frac{\partial f_1}{\partial x_2} & \cdots & \frac{\partial f_1}{\partial x_{2N}} \\ \frac{\partial f_2}{\partial x_1} & \frac{\partial f_2}{\partial x_2} & \cdots & \frac{\partial f_2}{\partial x_{2N}} \\ \vdots & \vdots & & \vdots \\ \frac{\partial f_{2N}}{\partial x_1} & \frac{\partial f_{2N}}{\partial x_2} & \cdots & \frac{\partial f_{2N}}{\partial x_{2N}} \end{bmatrix}, \tag{6}$$

This method can be applied to produce Variational Equations for any Continous Hamiltonian System. This method, however, will not work for Discrete Systems.

3.2 Tangent Map Method

Discrete dynamical systems are mappings with a general form shown in equation 7 where $f : M \to M$ maps a point in space M to another point in Space M.

$$x_{n+1} = f(x_n) \geq 0 \tag{7}$$

These systems will map points on a manifold from one location to another over time, hence they are also known as Maps (Strogatz & Dichter, 2016). Maps are often easier to compute and evolve. Symplectic Maps are used to evolve initial conditions of a system by one timestep. These area-preseving Maps often arise in Hamiltonian Dynamics, hence the need to study them (Meiss, 2008). Symplectic maps are often used in place of continuous Hamiltonians, since they are easier to compute and analyse. A simple symplectic map is shown in equation (8).

$$x_{t+1} = Sx_n \tag{8}$$

where x is the position vector of a system. The Tangent map can be produced by taking a partial derivative of the Symplectic map with respect to some variable. These tangent mappings do not produce variational equations since the Tangent Map is iterated to evolve $\overrightarrow{v}$, not integrated. This method will produce a *Differential* (Tangent) Map that can be iterated to evolve the deviation vector over time. The general form of a Tangent Map is shown in equation 9.

$$v(N+1) = \left.\frac{\partial S}{\partial x}\right|_N v(N) \tag{9}$$

where $T = \left.\frac{\partial S}{\partial x}\right|_N$ is a Tangent Map of a system iterated N times. The Tangent Map can be written in Matrix form which is shown in equation 10. where n corresponds to the number of variables in the Symplectic Map S.

$$T = \begin{bmatrix} \frac{\partial S_1}{\partial x_1} & \frac{\partial S_1}{\partial x_2} & \cdots & \frac{\partial S_1}{\partial x_n} \\ \frac{\partial S_2}{\partial x_1} & \frac{\partial S_2}{\partial x_2} & \cdots & \frac{\partial S_2}{\partial x_n} \\ \cdots & \cdots & \cdots & \cdots \\ \frac{\partial S_n}{\partial x_1} & \frac{\partial S_n}{\partial x_2} & \cdots & \frac{\partial S_n}{\partial x_n} \end{bmatrix} \tag{10}$$

The Tangent Map in this form can be applied to any deviation vector v where v is rewritten as a column matrix. The Deviation vector provides information on nearby trajectories in a system and how they behave relative to each other. The Deviation vector is an important component in any chaos indicator since one of the criterion for trajectories to be chaotic is based on its' relation to nearby orbits.

4 Chaos Indicators

4.1 Maximal Lyapunov Exponent

Maximal Lyapunov Characteristic Exponent is a chaos indicators that quantify the average rate of change of small perturbations to the solutions of dynamic systems (Benettin et al., 1980). The concept of Lyapunov Exponents was first introduced in 1892 by Lyapunov himself and have now been widely used to study the behaviour of dynamical systems (Benettin et al., 1980). The Maximal Lyapunov Exponent X_1 has two forms. The first form is known as the finite time mLCE X_1, which is computed using the formula shown in equation (11).

$$X_1 = \frac{1}{t} ln \frac{||v(t)||}{||v(0)||} \tag{11}$$

The finite-time mLCE is an easily computable quantity, however it fails to predict the long-term behaviour of trajectories. The true mLCE corrects this by taking $\lim_{t\to\infty}$ of the finite-time mLCE. The true mLCE is computed using the equation shown below.

$$\chi_1 = \lim_{t\to\infty} X_1 \tag{12}$$

We can rewrite the mLCE in integral form by using identity 13. This is done so that MEGNO and the mLCE can be compared.

$$\int \frac{f'(x)}{f(x)} dx = ln(f(x)) \tag{13}$$

Applying identity 13 to equations 11 and 12 allows us to rewrite both the finite and true mLCE in integral form. The δ in the equations are functions of the deviation vector v and its' Euclidean norm. The Euclidian norms of v and its' derivative are shown in equation 14. This notation will be carried through the rest of the report.

$$\begin{aligned} \delta &= ||v(t)|| \\ \dot{\delta} &= \dot{v} \cdot \frac{v(t)}{||v(t)||} \end{aligned} \tag{14}$$

Equation 15 shows the finite and true mLCE in Integral form, where $\cdot$ denotes inner product. $\dot{v}$ is the derivative of the deviation vector, typically attained by using Variational Equations.

$$\begin{aligned} X_1(\varphi(t)) &= \frac{1}{t} \int_0^t \frac{\dot{\delta(s)}}{\delta(s)} ds \quad = (\overline{\frac{\dot{\delta}}{\delta}}) \\ \chi(\varphi(t)) &= \lim_{x\to\infty} X_1(\gamma) \end{aligned} \tag{15}$$

The integral form of the mLCE defines it as the average of the change in the deviation vector over the deviation vector itself. The mLCE for a regular trajectory will $\to$ 0 after a sufficiently long time period. It is often computationally impossible to evolve a trajectory until its mLCE is 0. We will therefore consider trajectories with a sufficiently small mLCE that continues to decay as regular. mLCE that do not decay towards zero reflect chaotic trajectories, even if the mLCE value itself is small.

4.2 Fast Indicators and the FLI

The Lyapunov Exponents for many systems are estimated using numerical methods and are often only considered accurate after long time periods t. Fast indicators also known as finite time chaos indicators are known to be able to differentiate between regular and chaotic trajectories in times less than t (Lega et al, 2016). One of the first Fast indicators produced was the Fast Lyapunov Indicator (FLI) which was developed in 1997 (Lega & Froeschle, 1997). The FLI is shown in equation 16.

$$FLI = ln(\delta(\varphi(t))) \tag{16}$$

The deviation vector can contain lots of information about the system even over shorter time periods. The computation of the mLCE depends on both the deviation vector and its' rate of change. The rate at which the deviation vector grows/shrinks varies over time, hence the mLCE is often integrated over long times so its' true value (12) can be accurately approximated. The FLI, however, does not depend on the rate of change of the deviation vector. The FLI can therefore be approximated using shorter time periods since it depends only on the deviation vectors. The FLI will grow exponentially as $t \to \infty$ if the orbits are chaotic, and grow linearly if the system is regular. The time average FLI is written as equation 17 which computes the running average of the FLI values from time 0 to time t (Cincotta & Giordano, 2016).

$$\bar{FLI} = \int_0^t ln(\delta(\varphi(t)))ds \tag{17}$$

Although the FLI can detect chaos over less timesteps than the mLCE, some of its' parameters must be chosen carefully for it to work (Lega et al,). The initial deviation vector $v(0)$ must be chosen with care since it can blow up the FLI in some cases. THe integration time t must also be chosen carefully since the FLI will grow as $t \to \infty$ regardless of the behaviour of the Orbit. We will now present a new Fast Indicator, that does not have such restrictions but also performs well over shorter time periods (relative to the mLCE).

5 Theory of MEGNO

The Mean Exponential Growth Factor of Nearby Orbit (MEGNO) was first proposed by Nunez et al in 1997, however it was only fully developed and generalised in 2003 by Cincotta et al where its form for both discrete and continous systems was described. Since then, it has been used largely in astrophysics as shown in several papers referenced in Maffione et al (2011). In this section we will outline the theory of MEGNO as well as its' expected behaviour in chaotic and regular systems.

MEGNO can be considered a weighted variant of the mLCE. (Maffione et al, 2011). It is thus extremely similar to the mLCE in integral form. The formula used to compute MEGNO is shown below:

$$Y(\varphi(t)) = \frac{2}{t}\int_0^t \frac{\delta(\dot{\varphi(s)})}{\delta(\varphi(s))}sds \tag{18}$$

MEGNO computes the average value of the function $f = \frac{\delta(\dot{\varphi(t)})s}{\delta(\varphi(t))}$ multiplied by two. The function f is numerically integrated using any method in order to compute MEGNO. We will illustrate how MEGNO acts as a chaos indicator. One of the objectives of MEGNO was to enhance the exponential sensitivity of chaotic orbits to initial conditions since this would produce a clear classification between chaotic, and regular orbits (Mestre et al, 2013). This is can be seen after shifting the system and MEGNO to action-angle variables (I, θ).

Action-angle variables are used to exploit Hamiltonian mechanics. These variables allow us to determine the frequency of periodic motion without using exact trajectories(Cline, 2021). We can define systems in terms of action-angle variables (I, θ) instead of (q, p). Consider an orbit $\varphi_q(t)$ on an irrational torus. For the sake of simplicity we will assume that the orbit exists in an isochronous[1] system. The local action angle variables can then be defined:

$$\begin{aligned} \theta(t) &= \omega(I)t + \theta_0 \\ I &= I_0 \end{aligned} \tag{19}$$

where ω defines the frequency of the orbits and action variable I is kept constant. Holding I constant will define the surface of a torus. We can now rewrite our deviation vector using (I, θ) shown in equation 20(Cincotta

[1]Isochronous systems are systems for which there exist an open set of initial conditions that will produce only periodic trajectories (Calogero, 2011)

& Giordano, 2016).

$$\delta(\varphi_q t) \approx \delta_0(1 + w_q(t) + t(\lambda_q + u_q(t))) \tag{20}$$

In equation 20, the functions w_q, u_q are oscillatory with $|u_q| \leq b_q < \lambda_q$ where b_q is some positive constant. $\lambda_q > 0$ is the rate of divergence around φ_q and consequently measures the presence (or lack) of isochronicity in a trajectory. If we substitute equation 20 into equation 18 we can verify that

$$|Y(\varphi_q(t)) - 2| \leq 4 \ln \frac{\lambda_q + b_q}{\lambda_q - b_q}, \quad t \to \infty \tag{21}$$

according to Cincotta & Giordano (2016). Y can be approximated by rewriting 21. This is shown in equation 22. The O in equation 22 refers to an oscillating term due to the functions w_q, u_q.

$$Y(\varphi_q(t)) \approx 2 - \frac{2 \ln(1 + \lambda_q t)}{\lambda_q t} + O(\varphi_q(t)), \tag{22}$$

$\lambda = 0$ for any regular trajectories since the divergence does not occur. The second term in equation 22 will disappear as $t \to \infty$ and Y will oscillate around 2. In order to see how MEGNO behaves, we can take its' limit as $t \to \infty$ as we did with the finite mLCE. However, since MEGNO oscillates, the limit of Y will not exist. We can thus compute the time average of Y, denoted $\bar{Y}$.

$$\bar{Y}(\varphi_q(t)) = \frac{1}{t} \int_0^t Y(\varphi_q(s)) ds \tag{23}$$

The Time average of MEGNO ($\bar{Y}$) will tend to 2 for regular trajectories whilst Y oscillates around 2. The oscillatory nature of Y can often create difficulties when analysing a system, thus $\bar{Y}$ is preferred when analysing orbits. If the Trajectories are non-regular, Y and $\bar{Y}$ will grow as $t \to \infty$.

5.1 MEGNO in General and for Maps

Equation 18 is a specific case of the MEGNO indicator. We can generalise it by introducing parameters (m, n) and rewriting equation 18 and 23 as shown in 24 according to Cincotta & Giordano (2016).

$$\begin{aligned} Y_{m,n}(\varphi(t)) &= (m+1)t^n \int_0^t \frac{\delta(\dot{\varphi(s)}) s^m}{\delta(\varphi(s))} ds \\ \bar{Y_{m,n}}(\varphi(t)) &= \frac{1}{t^{(m+n+1)}} \int_0^t Y_{m,n}(\varphi(s)) ds \end{aligned} \tag{24}$$

Both equations 18 and 23 show the MEGNO indicator when $(m, n) = (1, -1)$, however these parameters can be varied. The behaviour of Y and $\bar{Y}$ changes based on the values of (m, n). We can shift the deviation vector into action-angle variables as done in the previous section, substitute the shifted deviation vector into equation 24 and see how the resulting functions are related to (m, n). The full derivation of how to do this is shown in Cincotta and Giordano (2016). If the orbit φ is regular, $Y_{m,n}$ and $\bar{Y}_{m,n}$ will tend towards the values shown in equation **??** as $t \to \infty$.

$$\begin{aligned} Y_{m,n}(\varphi(t)) &\approx \frac{(m+1)}{m} \\ \bar{Y_{m,n}}(\varphi(t)) &\approx \frac{(m+1)}{m(m+n+1)} \end{aligned} \tag{25}$$

The Generalised MEGNO indicators can be related to the mLCE according to Cincotta and Giordano (2016). This relation is shown in equation 26 which shows that MEGNO will grow at a linear rate proportional to the mLCE of the chaotic orbit.

$$\begin{aligned} \frac{Y_{m,n}(\varphi(t))}{t^{m+n}} &\approx \chi \frac{(m+1)}{m} + O(\tilde{\varphi}(t)) \\ \bar{Y_{m,n}}(\varphi(t)) &\approx \frac{\chi t)}{(m+n+2)} \end{aligned} \tag{26}$$

Although larger m values will result in Y converging quicker, it will cause the greater oscillations in Y (Cincotta & Giordano, 2016). Therefore, the MEGNO indicator will use $(m, n) = (1, -1)$ in this report.

5.2 Relation between MEGNO and FLI

MEGNO and the Fast Lyapunov Indicator are both fast indicators. In this section we will show how they are related and consequently, why MEGNO performs better as a chaos indicator compared to the FLI. We begin by applying integration by parts [2] to the MEGNO formula in equation 18. We choose:

$$\begin{aligned} u &= s \\ dv &= \int \frac{\dot{\delta}(\varphi(s))}{\delta(\varphi(s))} \end{aligned} \tag{27}$$

Then 18 can be rewritten in terms of FLI as shown in equation 28.The logarithmic terms are obtained via the identity 13 after integrating by parts.

$$\begin{aligned} Y\left(\varphi(t)\right) &= \frac{2}{t}(t \cdot ln||\delta(\varphi(t))|| - \int_0^t ln||\delta(\varphi(s))||ds) \\ Y\left(\varphi(t)\right) &= 2(FLI - \bar{FLI}) \end{aligned} \tag{28}$$

The MEGNO provides a time-independent condition that differentiates between chaotic and regular orbits. This is due to MEGNO quantifying the degree of chaoticity on an absolute scale, whereas the FLI only provides relative values to compare one another to(Mestre et al, 2011). The MEGNO indicator provides a better criteria for chaos (or periodicity) compared to the FLI, making it a better chaos indicator.

6 Numerical Computation of MEGNO

All numerical computations in this report are done in Python 3.10. Computations of the Global Dynamics of Systems were done on the High Performance Computing Cluster (HPC) since these scripts are often computationally heavy. Computing the chaos indicator for a few trajectories is done using a local machine. The Scripts used can be found on the Github repository https://github.com/qiulinlx/MEGNO.

6.1 Continous Systems

The computation of MEGNO for continuous systems follows directly from its' formula shown in Equation 18. The computation requires that the Variational Equations of the system be written in Matrix form, as well as the Equations of motion of the system. If the system is chaotic, the deviation vector will grow as the trajectories evolve over time. A skeleton code for the computation of MEGNO is given in below.

[2] $\int u \cdot dv = uv - \int v \cdot du$

Skeleton code for the Computation of MEGNO $Y(N)$ for Continuous Systems
Input: Initial conditions x_i and initial Deviation vector v_i
Create empty lists $delta = []$, $Dotdelta = []$, $times = []$ and $xl = []$
For k in range (n):
$\longrightarrow$ Evolve orbit $x_k(k\tau)$ and deviation vector $v_k(k\tau)$ over timestep τ to x_{k+1}, v_{k+1} *
$\longrightarrow$ Append $k\tau$ to list $times$
$\longrightarrow$ Compute $\dot{v_{k+1}}(k\tau)$ via $\Lambda \cdot v_{k+1}$
$\longrightarrow$ Compute $\delta = \|\|v_{k+1}(\tau)\|\|$
$\longrightarrow$ Compute $\dot{\delta} = \dot{v_{k+1}} \cdot \frac{v_{k+1}}{\delta}$
$\longrightarrow$ Append δ to list $delta$ and $\dot{\delta}$ to list $Dotdelta$
$\longrightarrow$ Renormalise v: $v_k = \frac{v_{k+1}}{\delta}$
$\longrightarrow$ Preparation for next iteration: $x_k = x_{k+1}$
Create empty list $alpha = []$
For i in Range(len($delta$)):
$\longrightarrow$ Compute $\alpha = ln(\frac{Dotdelta[i]}{delta[i]})$
$\longrightarrow$ Append α to list $alpha$
Create empty list $MEGNO = []$
for i in range(N):
$\longrightarrow$ Compute $m = \frac{2}{i}$ auc($times[:i], alpha[:i]$) **
$\longrightarrow$ Append m to list $MEGNO$

The integral in equation 18 is computed in ** using the *auc* function. It is imported from the Scilearn package and approximates integrals by calculating the area under a curve using the trapezoidal rule. The trajectory and deviation vectors can be evolved by solving the equations of motion and variational equations using any numeric integrator. Non-symplectic integrators such as Runge-Kutta 4 and the DOP853 can be used by importing the *solve_ivp* function from the Scipy Package (Virtanen et al, 2020). Alternatively Symplectic methods can be used to evolve the system. These must be built in python explicitly, since there is no prebuilt package for symplectic integrators. Although the symplectic method requires more computation, it is recommended due to its' quicker computational time and high accuracy. The time evolution of the orbit and its deviation vectors occurs in *.

The list $MEGNO$ will consist of the $Y(N)$ values for $N = 1, 2....n$ which can be plotted to see how the MEGNO indicator performs over time. These values can also be used to find $\bar{Y}(N)$. This can be done using teh skeleton code shown below. Note that it requires the list of Y values in list $MEGNO$ from the Skeleton Code above.

Skeleton code for the Computation of average MEGNO $\bar{Y}(N)$ for Continuous Systems
Input: List $MEGNO$ with $Y(N)$ values and List $times$ with $k\tau$ vaules
Create empty lists $avmeg = []$
For k in range (n):
$\longrightarrow$ Compute $a = auc(times[:k], MEGNO[:k])$
$\longrightarrow$ Compute $av = \frac{a}{times[k]}$
$\longrightarrow$ Append av to list $avmeg$

The list $avmeg$ will have the $\bar{Y}(N)$ values for when $N = 1, 2...n$. The $Y(N)$ and $\bar{Y}(N)$ values are fairly straightforward to compute from the formula for MEGNO shown in equation 18. One of the condition to use this formula is that there exists a matrix that will allow us to compute $\dot{\delta}$. This is not the case with Discrete systems, thus another formula is required.

6.2 Discrete Systems

MEGNO for Maps are computed using a different formula, since Maps do not have variational equations. The equation which we use to compute MEGNO for Discrete systems is given in general in equation 29 and the specific one used in this report is shown in equation 30 where $m, n = (1, -1)$

$$\begin{aligned} Y_{m,n}(N) &= (m+1)N^n \sum_{k=1}^{N} \ln\left(\frac{\|\mathbf{v}_k\|}{\|\mathbf{v}_{k-1}\|}\right) k^m, \\ \bar{Y}_{m,n}(N) &= \frac{1}{N^{m+n+1}} \sum_{k=1}^{N} Y_{m,n}(k). \end{aligned} \tag{29}$$

$$\begin{aligned} Y(N) &= \frac{1}{N} \sum_{k=1}^{N} \ln\left(\frac{\|\mathbf{v}_k\|}{\|\mathbf{v}_{k-1}\|}\right) k, \\ \bar{Y}(N) &= \frac{1}{N} \sum_{k=1}^{N} Y(k). \end{aligned} \tag{30}$$

The Symplectic and Discrete Tangent Map of the discrete system are required for the computation of MEGNO. The method of computing MEGNO is shown below where the final list *meg* consists of the $Y(N)$ values as the map is iterated $N = 1, 2...n$ times

Skeleton code for the Computation of MEGNO $Y(N)$ for Discrete Systems
Input: Initial conditions x_i and initial Deviation vector v_i Create empty lists $delta = []$, $times = []$ and $xl = []$
For k in range (n): $\longrightarrow$ Iterate orbit x_k and deviation vector v_k over Symplectic and tangent map respectively to x_{k+1}, v_{k+1} $\longrightarrow$ Compute $\delta = \|\|v_{k+1}\|\|$ $\longrightarrow$ Append δ to list $delta$ $\longrightarrow$ Renormalise the deviation vector via $v_k = \frac{v_{k+1}}{\delta}$
Remove first value in $delta$ (Erronous) $\longrightarrow$ Compute new list of lnδ values $ld = ln(delta)$
Create new empty list $zz = []$ For i in range (len(ld)): $\longrightarrow$ Compute $z = i \times ln[i]$ $\longrightarrow$ Append z to list zz
Create new empty list $meg = []$ For i in range(len(zz)): $\longrightarrow$ Compute $m = \frac{2}{i} sum(zz[:i])$ $\longrightarrow$ Append m to list zz

The computation of MEGNO for Discrete systems may appear easier than its' computation for continous systems since it does not require systems to be numerically integrated. It also does not use the *auc* function since it is not necessary to approximate the area under a curve. The computation of the time average of MEGNO ($\bar{Y}$), can be computed using the Y values in a single loop.

Skeleton code for the Computation of average MEGNO $\bar{Y}(N)$ for Discrete Systems
Input: List meg with $Y(N)$ values a Create empty lists $avmeg = []$ For i in range (len(meg)): $\longrightarrow$ Compute $yb = \frac{sum(meg[:i])}{i}$ $\longrightarrow$ Append yb to list $avmeg$

THe final list *avmeg* will be made up of the $\bar{Y}$ values, which reflect the running time average of MEGNO as it continously iterates. The method of computing MEGNO for continous and discrete systems has now been described in this section. We can now apply these methods to continous and discrete systems to verify the behaviour of MEGNO as a fast chaos indicator.

7 Application to Henon-Heiles

The Henon-Heiles Hamiltonian was produced by looking at galactic motion (Henon & Heiles, 1964)). It is an autonomous Hamiltonian that has been widely studied in relation to dynamics and chaos. The Hamiltonian H, is shown in equation 31.

$$H = \frac{1}{2}(p_x^2 + p_y^2) + \frac{1}{2}(x^2 + y^2) + x^2 y - \frac{1}{3}y^3 \tag{31}$$

The Henon-Heiles Hamiltonian conserves the total energy in a system. which can vary from $E = 0$ to $E = \frac{1}{6}$. Variations in the total energy of the system E will produce trajectories that are either chaotic or regular. The position and momentum coordinates of the system are evolved over time via the equations of motion of the Henon-Heiles system shown below.

$$\begin{cases} \dot{x} = p_x \\ \dot{y} = p_y \\ \dot{p_x} = -x - 2xy \\ \dot{p_y} = -y - x^2 + y^2 \end{cases} \tag{32}$$

If we evolve the Henon-Heiles system while varying the initial conditions and energy levels, both regular or chaotic trajectories will emerge. This evolution is done using the $SABA_2C$ symplectic integrator. The differential operators used in symplectic integrators for the Henon-Heiles system is shown below.

$$L_A = \begin{cases} x = x + p_x\tau \\ y = y + p_y\tau \\ p_x = p_x \\ p_y = p_y \end{cases} \tag{33}$$

$$L_B = \begin{cases} x = x \\ y = y \\ p_x = p_x - x(1 + 2y)\tau \\ p_y = p_y + (y^2 - x^2 + y)\tau \end{cases} \tag{34}$$

$$e^{L_C\tau} = \begin{cases} x = x \\ y = y \\ p_x = p_x - 2(1 + 2x^2 + 6y + 2y^2)\tau \\ p_y = p_y - 2(y - 3y^2 + 2y^3 + 3x^2 + 2x^2 y)\tau \end{cases} \tag{35}$$

Poincare surface sections are commonly used to visualise chaotic orbits (Strogatz & Dichter, 2016). These are sections that show how a trajectory is evolving in Phase space. We will therefore use these graphs to visualise the trajectory for some initial conditions (y, p_y) after setting $x = 0$. Using the initial conditions and $x = 0$, we can calculate p_x using the equation shown below.

$$p_x = \sqrt{2H - p_y^2 - y^2 + \frac{1}{3}y^3} \tag{36}$$

Given $E = \frac{1}{8}$, the Henon-Heiles system will show both regular, chaotic and sticky trajectories. A Poincare surface section of this system is shown in Figure 3. The figure shows multiple initial conditions evolved over 5000 timesteps where each step $\tau = 0.05$.

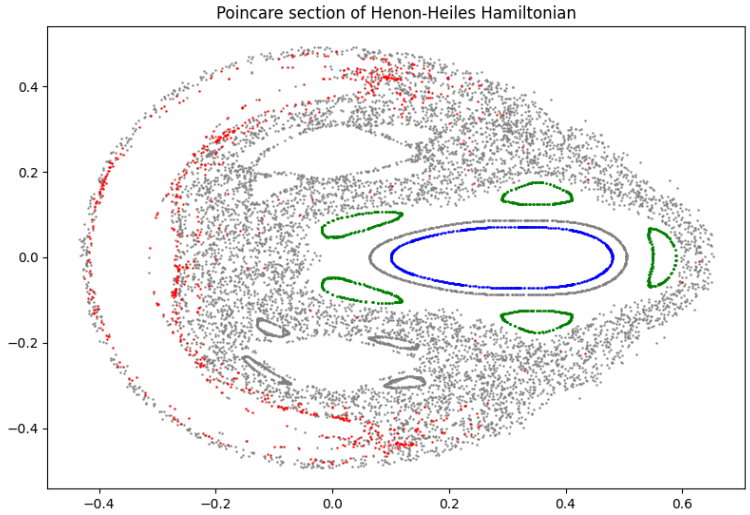

Figure 3: Poincare Section of Henon-Heiles system with multiple initial conditions iterated over 5000 timesteps.

The trajectories highlighted using non-grey points have a different behaviour that will be analysed. The initial conditions and behaviour of each trajectory is shown in the table below along with the colour which will be used to represent it in this analysis. The regular orbit is blue in 3, the chaotic one is red and the sticky orbit is green. These colourings will be correspond to the respectic behaviours in this report. [3]

Behaviour	Energy	Initial Conditions (y, py)	Colour
Regular	$\frac{1}{8}$	(0.1, 0)	Blue
Chaotic	$\frac{1}{8}$	(-0.25, 0)	Red
Sticky	$\frac{1}{8}$	(0.55, 0)	Green

The mLCE and MEGNO indicator for the Henon-Heiles system can be calculated and compared for the sticky, regular and chaotic trajectory. Both computations require the evolution of the Trajectory and its deviation vector. The evolution of the trajectory can be done by solving the equations of motion of the system. The evolution of the deviation vector is done by integrating the Variational Equations. The variational equations in Matrix form is shown in equation 37.

$$\Lambda = \begin{bmatrix} 1+2y & 2x & 0 & 0 \\ 2x & 1-2y & 0 & 0 \\ 0 & 0 & 1 & 0 \\ 0 & 0 & 0 & 1 \end{bmatrix} \tag{37}$$

The equations of motion and the variational equations are solved via the symplectic integration scheme $SABA_2C$ shown in equation 38. This is a Symplectic integration scheme of order 4 that is often used for its simplicity and accuracy. The full integration scheme is described in this paper (Laskar Robutel, 2003).

$$SABA_2C(\tau) = e^{L_H} = e^{\frac{c}{2}\tau^3 L_C} e^{c_1 \tau L_A} e^{d_1 \tau L_B} e^{c_2 \tau L_A} e^{d_1 \tau L_B} e^{c_1 \tau L_A} e^{\frac{c}{2}\tau^3 L_C} \tag{38}$$

The chaos indicators MEGNO and mLCE are used to evaluate the sticky, regular and chaotic orbit. A comparison of the two indicators is shown in Figure 4a. Both indicators evolve the trajectories for 500 timesteps with $\tau = 0.1$.

[3] All analysis of sticky orbits are green, all analysis of regular orbits are blue etc.

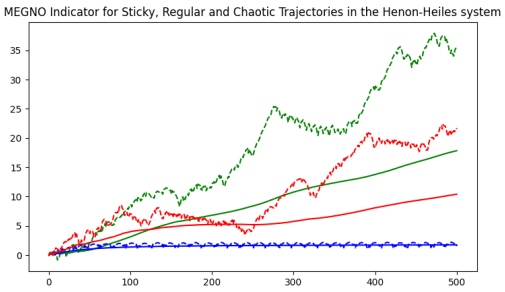

(a) MEGNO Indicator

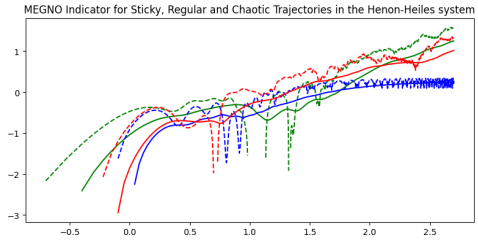

(b) Log10(MEGNO) Indicator

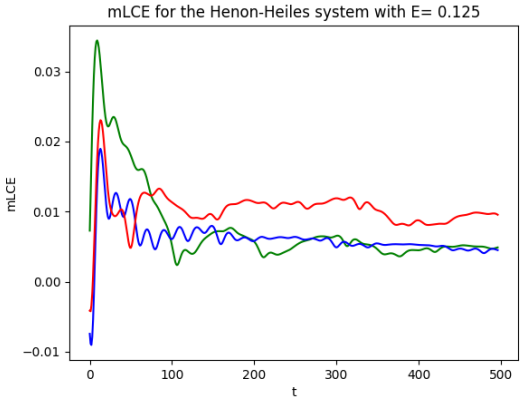

(c) mLCE

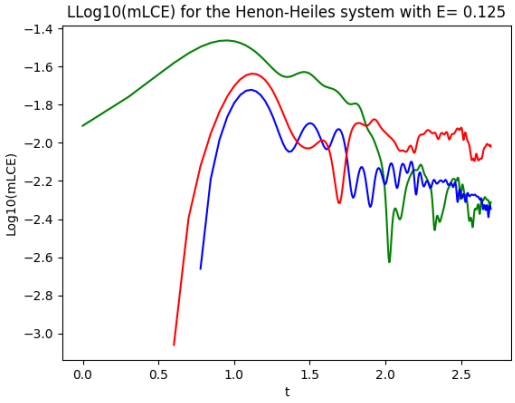

(d) Log10(mLCE) Indicator

Figure 4: Comparison of chaos indicators

The MEGNO differentiates between chaotic and regular trajectories more clearly compared to the mLCE. The mLCE values all tend to be less than 1, which means differentiating between the different trajectories will be difficult. The $Y(N)$ values represented by the dashed lines in figure 4a tend to oscillate as time progresses. $\bar{Y}(N)$ represented by the solid line shows the non-oscillatory version of MEGNO. The MEGNO indicator illustrates that the Green orbit is chaotic whereas the mLCE shows that it is regular. In Figure 3, we evolved each orbit for 5000 timesteps. A plot of the evolution of the green orbit for longer periods (5000000 timesteps) is shown in Figure 5

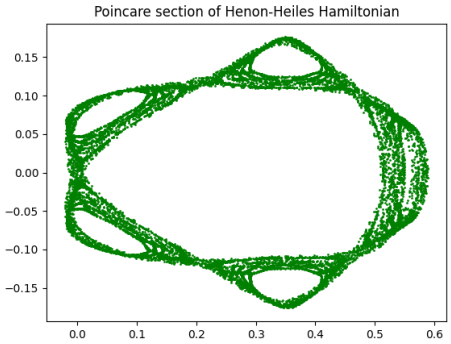

Figure 5: Poincare Section of a Sticky orbit in the Henon-Heiles system

The original cantori merge and the interact, indicating that the Orbit is Sticky. Since Sticky orbits are considered Chaotic, the MEGNO Indicator correctly identified the behaviour of the trajectory within 500 timesteps. The mLCE fails to identify the behaviour of this orbit in 500 timesteps, however, it will succeed in correctly identifying the orbit after 2000 timesteps as shown in the figure below. as the mLCE for the sticky orbit does

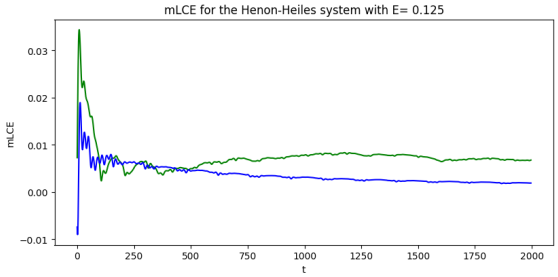

Figure 6: mLCE of Sticky Orbits

not decay and is larger than the mLCE for the regular orbit.

8 Application to 2D Standard Map

The 2D Standard map is an area-preserving map that is commonly studied in relation to non-integrable Hamiltonian systems (Tobin, 2009). It is also known as the Chirikov map that arises in several different contexts, such as a kicked periodic oscillator (Strogatz & Dichter, 2016). One common form of the 2D Standard map is shown below. It should be noted that this is one of several forms of this standard map.

$$\begin{aligned} x_1' &= x_1 + x_2' \qquad\qquad (mod 2\pi) \\ x_2' &= x_2 + \frac{K}{2\pi} sin(2\pi x_1) \quad (mod 2\pi) \end{aligned} \tag{39}$$

x_1 and x_2 can be considered the position and momentum of the trajectory. The map evolves the trajectory by one step in Phase space for every iteration of the map. $x'_{1,2}$ denotes the coordinates of the system after the current iteration of the mapping.

The parameter K in equation 39 can be varied . The 2D Standard Map will produce both chaotic and regular trajectories based on the value of parameter K. Only non-negative K values are considered since negative K provides the same trajectories as positive K ((Tobin, 2009)). We know that for small K, the system will only produce Regular trajectories. Similarly if we have an extremely large K, we will only produce chaotic trajectories. K will thus be set to 0.8 so chaotic, regular and sticky trajectories can emerge. The general PSS of the 2D Standard Map when $K = 0.8$ is shown in Figure 7.

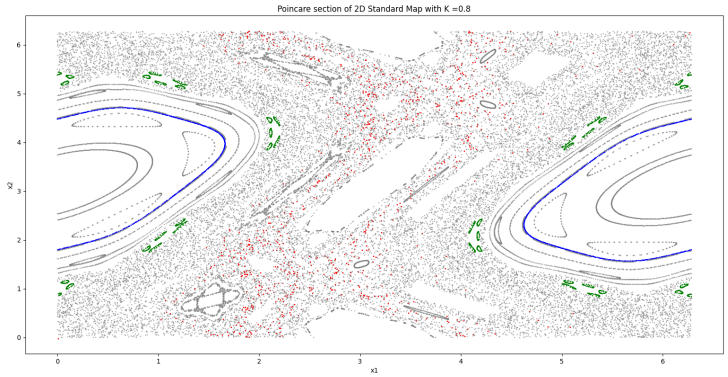

Figure 7: Poincare Section of 2D Standard Map with multiple initial conditions iterated over 500 timesteps.

The initial conditions for sticky regular and chaotic trajectories are chosen by picking values in the regular

islands, chaotic regions and the areas where cantori are present. The following values are chosen as initial conditions for regular, chaotic and sticky orbits.

Behaviour	K	Initial Conditions $(x1, x2)$
Regular	0.8	(1.65, 3.86)
Chaotic	0.8	(0.01, -0.02)
Sticky	0.8	(0.038, 0.9)

We can analyse these orbits using both MEGNO as well as the mLCE. The computation of both of these indicators require the use of the Differential Tangent Map of the 2D Standard Map. The Differential Map is written out in matrix form in equation 40.

$$T = \begin{bmatrix} 1 + Kcos(2\pi x_1) & 1 \\ Kcos(2\pi x_1) & 1 \end{bmatrix} \tag{40}$$

Applying the Differential Map to some initial deviation vector v will evolve the vector over tangent space and allow us to compute the deviation vector over time. After finding the deviation vector after various iterations, we can substitute it into equation 30 to compute MEGNO. The behaviour of MEGNO is shown in Figure 8a.

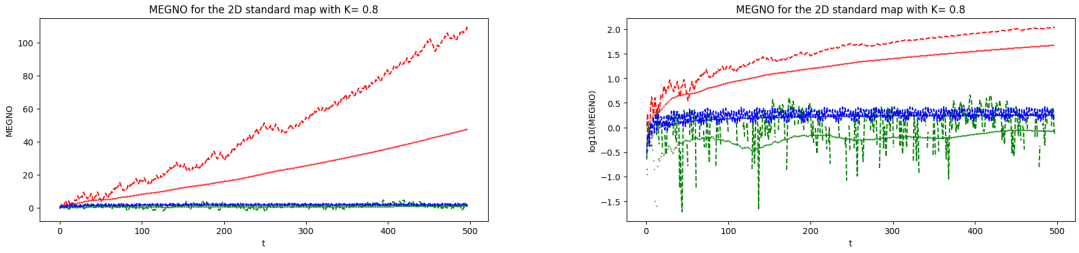

(a) MEGNO Indicator

(b) Log10(MEGNO) Indicator

Figure 8: MEGNO indicator

The MEGNO indicator classifies the Sticky orbit as regular if the trajectory is only evolved for 500 timesteps. The Indicator will however grow exponentially for chaotic trajectories. In order to illustrate that the green trajectory is sticky, we can evolve its' MEGNO indicator over 50000 timesteps. This MEGNO plot in figure 9a shows that the Green Orbit is indeed sticky since the Y and $\bar{Y}$ value of the green orbit does not stay constant and eventually grows.

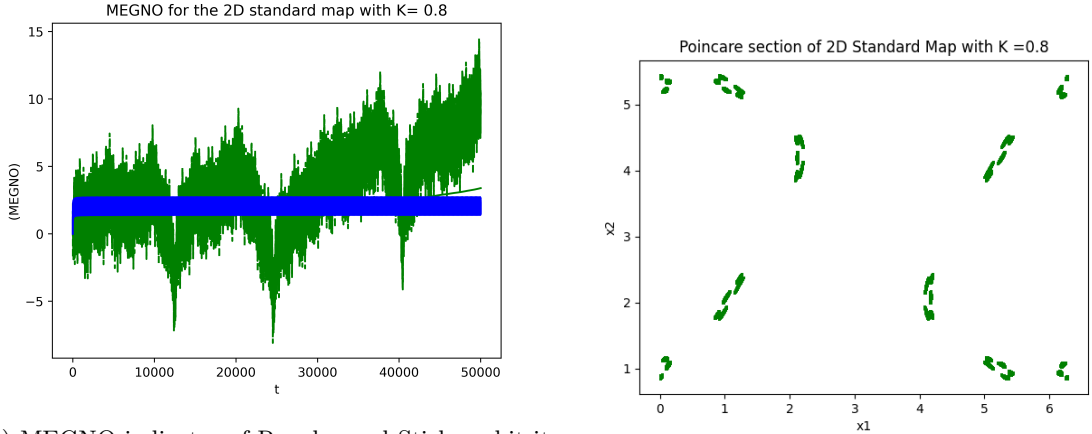

(a) MEGNO indicator of Regular and Sticky orbit iterated over 50000 steps

(b) Sticky orbit of 2D Maps

This illustrates that the Sticky orbit can be distinguished by the MEGNO indicator after the trajectory has been iterated over 5000 steps. The plot of the sticky orbit in the 2D map after 50000 iterations is shown in Figure 9b. The stickiness of the orbit has not emerged after 50 000 iterations. This is consistent with the findings from applying MEGNO to the Henon-Heiles system, since MEGNO can show that an orbit is sticky, before the orbit begins showing its sitcky behaviour. The mLCE of the 2D Map iterated over the 500 and 50000 steps is shown in Figure 10. The fact that the mLCE is still tending to 0 at 50000 iterations indicates that stickiness should not emerge yet at that point.

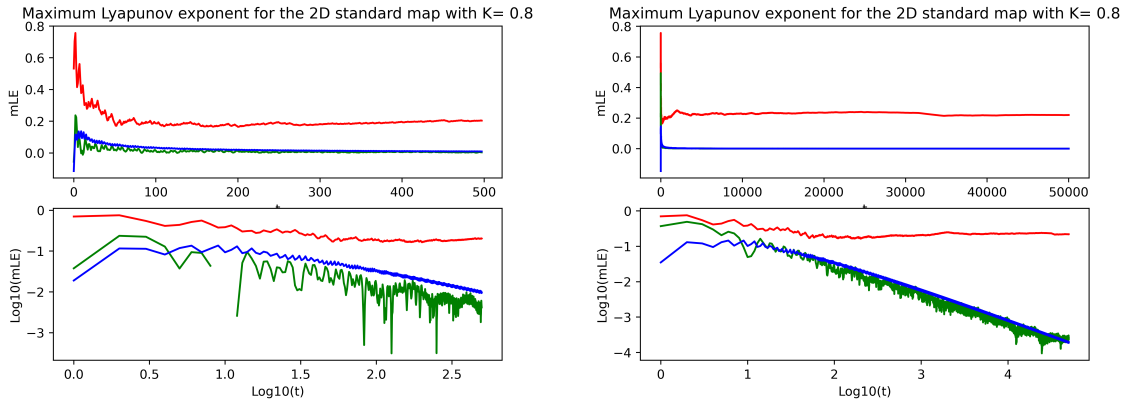

(a) mLCE over 500 steps

(b) mLCE over 50000 steps

Figure 10: mLCE over 50000 steps

Figure 10 shows that the mLCE will classify the Green orbit as Regular since the mLCE value of the regular (blue) orbit and the mLCE of the green orbit are extremely similar. Although the mLCE can correctly differentiate between standard regular and chaotic trajectories, it fails to classify the sticky orbit as chaotic.

9 Application to 4D Standard Map

Coupling together two 2D Standard Maps will produce the 4D Standard Map. The Mapping is shown in equation (41) where x_1, x_3 are the position and x_2, x_4 are momenta of the system.

$$\begin{aligned} x_1' &= x_1 + x_2' \\ x_2' &= x_2 + \frac{K}{2\pi}\sin(2\pi x_1) - \frac{B}{2\pi}\sin\left[2\pi\left(x_3 - x_1\right)\right] \quad (\mathrm{mod} 1). \\ x_3' &= x_3 + x_4' \\ x_4' &= x_4 + \frac{K}{2\pi}\sin(2\pi x_3) - \frac{B}{2\pi}\sin\left[2\pi\left(x_1 - x_3\right)\right] \end{aligned} \tag{41}$$

where K, B are parameters to be set arbitrarily. The 4D map has many unique dynamical properties that are beyond the scope of this report. Further details on this map (41) can be found in (Kantz & Grassberger, 1988) where it was originally described. B is the Coupling factor that causes the trajectories of the two 2D Maps to interact since turning B off will cause the two maps to stop interacting. The K parameter in equation 41 is similar to the one that appears in the 2D Standard Map. For the 2D Standard Map, $K = 0.8$ will provide chaotic and regular orbits. We will thus keep K at this value and reduce coupling by setting $B = 0.1$.

The 4D Standard Map with $K = 0.8$ and $B = 0.1$ will produce regular, chaotic and sticky orbits. (these ICS are found experimentally by exploring the global dynamics of the system) The initial conditions that will produce the various behaviours of the system is shown below.

Behaviour	K	B	Initial Conditions $(x1, x2, x3, x4)$
Regular	0.8	0.1	$(0.2, 0.1, 0.21, 0.1)$
Chaotic	0.8	0.1	$(0.01, 0.02, 0.01, 0.02)$
Sticky	0.8	0.1	$(0.46, 0.1, 0.21, 0.1)$

The 4D map (obviously) occurs in 4 Dimensions, which is difficult to visualise in 2D Poincare Sections. We will visualise the orbits by plotting $(x1, x2, x3)$ over time and show $x4$ as a colour gradient. The resulting plots are shown in Figure 11a, 12a and 13a. Since $(x1, x2)$ are the variables of one of the two coupled Maps, we can use visualise the evolution of the one coupled map in 2D.

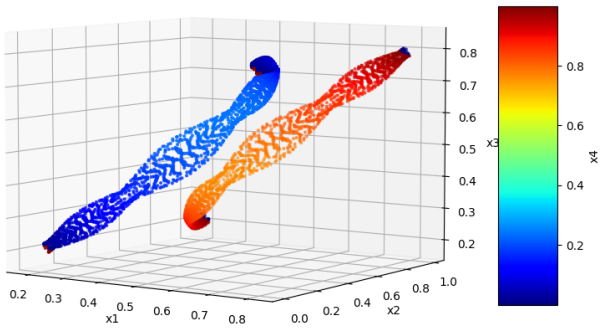

(a) Phase Space portrait of Regular orbit in 4D Map.

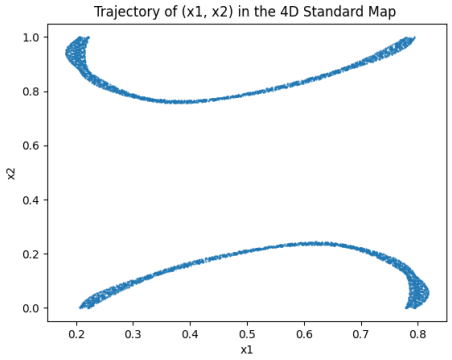

(b) Trajectory of $(x1, x2)$ of 4D Map.

Figure 11a show that the system is regular since the 3D structure and colour gradient illustrate some underlying structure. Figure 11b shows that the $(x1, x2)$ themselves also behave regularly. Disturbances from the coupling are relatively small since $B = 0.1$.

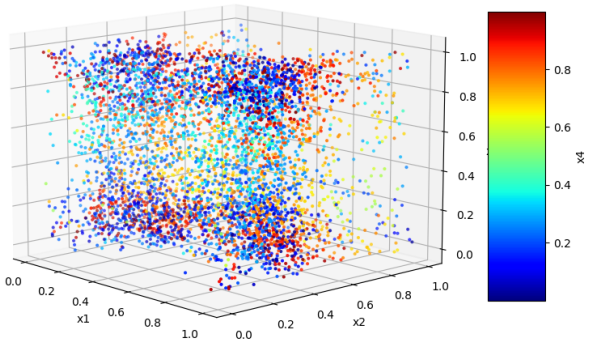

(a) Phase Space portrait of Chaotic orbit in 4D Map.

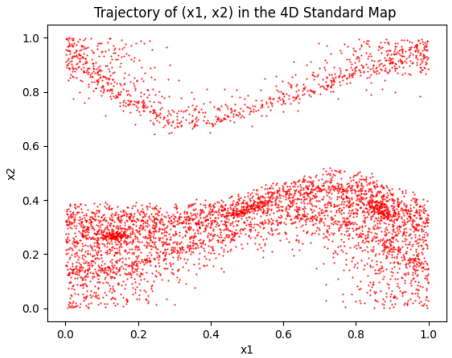

(b) Trajectory of $(x1, x2)$ of 4D Map.

Figure 12a show that the system is chaotic since the 3D structure has no structure, regardless of the colour gradients of these structureless points. Figure 12b shows that for Chaotic orbits, the $(x1, x2)$ points will diffuse into nearby areas, depicting chaos.

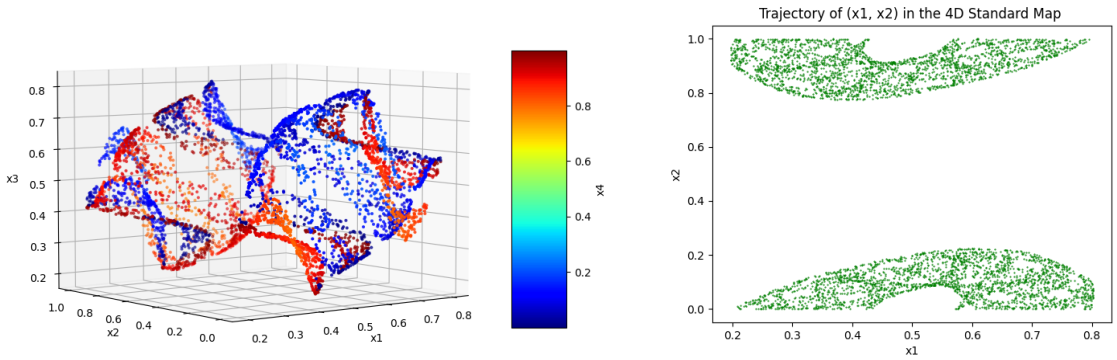

(a) Phase Space portrait of Sticky orbit in 4D Map.

(b) Trajectory of $(x1, x2)$ of 4D Map.

Figure 13a shows a structure that is somewhere in between Figure 11a and 12a. Some points are ordered, however there are also many that are not. Figure 13b shows the the points $x1, x2$ will still diffuse into nearby areas when the orbit is sticky, however the Diffusion area is bounded implying some sort of structure. We can now use MEGNO as well as the mLCE to anaylse the behaviour of the three trajectories shown above. Computing thr MEGNO indicator for the three trajectories produces Figure 14a. The MEGNO indicator for the Chaotic Trajectory will grow linearly as the Map continuously iterates over itself. The Indicator does not grow after and oscillates around a set value (2) for the regular trajectory.

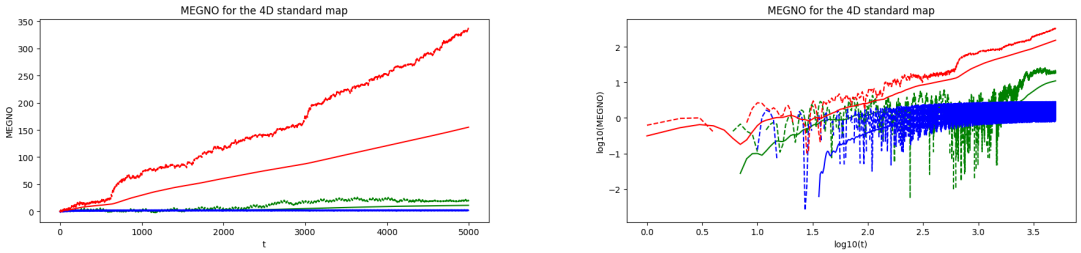

(a) MEGNO indicator

(b) Log10(MEGNO) Indicator

Figure 14: MEGNO indicator

The MEGNO indicator can successfully differentiate between chaotic and regular trajectories in the 4D Map. It also allows us to deduce that the green orbit is sticky, since it stays constant for a period, before growing slowly over the threshold value 2. The mLCE can similarly be used to differentiate between regular and chaotic orbits. The mLCE of the three trajectories of the 4D Map are shown in figure 15.

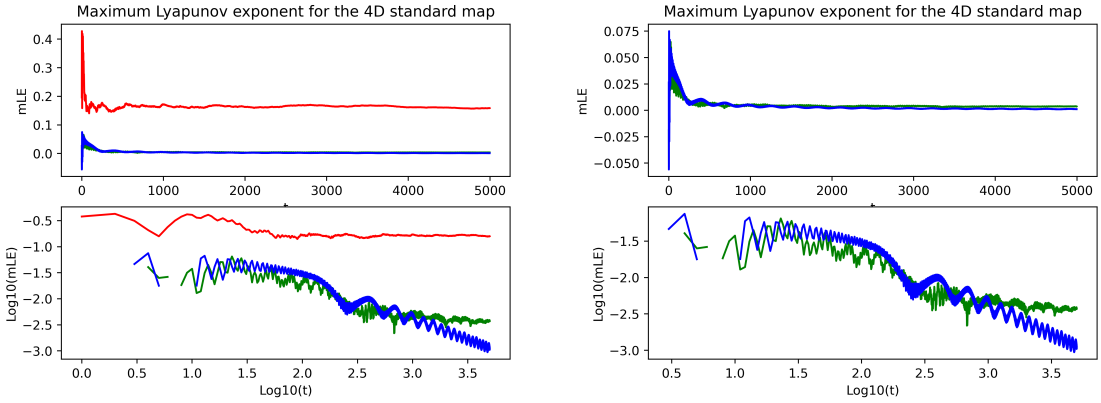

(a) mLCE indicator

(b) mLCE Indicator

Figure 15: mLCE indicator

The mLCE can similarly differentiate betwen sticky and regular orbits, however this can only be seen when studying the $log10(mLCE)$ values of these orbits. Both MEGNO and the mLCE can differentiate between chaotic, sticky and regular trajectories, however the distinction between regular and sticky orbits is clearer when MEGNO is used.

10 Global Dynamics

Chaos Indicators can be used to study the global dynamics of systems by telling us how many chaotic trajectories exist, relative to regular ones. This gives us a measure of how chaotic a system is. A system may be more chaotic than another, if it's ratio of chaotic to regular trajectories is larger than another (Strogatz & Dichter, 2016). This 'degree of chaos' can be inferred by applying Chaos indicators to the Global dynamics of a system. In this section we will compare the performance of MEGNO and the mLCE in quantifying the degree of chaos in system.

Chaos indicators are, however, not perfect and may misidentify the behaviour of these trajectories. Several different Trajectories with varying behaviours can be evolved and the chaos indicator for these trajectories can be computed. A comparison of the trajectories actual behaviour and its' behaviour according to the chaos indicator will show how accurately a indicator classifies the behaviour of an orbit.

The mLCE is a common chaos indicator that can be used to study the Global Dynamics of a system. The mLCE will classify trajectories as regular if

1. The mLCE value is sufficiently small enough
2. The log10(mLCE) decays over time

When we apply the mLCE to several trajectories, we only consider its' final value when the trajectory has finished evolving. This means we only have a single criteria to classify the trajectory. This criteria is imprecise, since the decision of what is considered sufficiently small is often implied and not explicitly stated. The MEGNO indicator, however, does provide a specific criteria for chaos.

The MEGNO indicator consists of an oscillatory value Y and a constant value $\bar{Y}$. Since $\bar{Y} \to 2$ for regular trajectories (Cincotta & Giordano, 2016). Any trajectories satisfying equation 42 is considered regular.

$$log10(\bar{Y}) < log10(\bar{Y}) = 0.301 \tag{42}$$

42 serves as a Criteria for which we can use to explicitly classify trajectories as chaotic or regular. Since $\bar{Y}$ grows exponentially for chaotic trajectories, the difference between the $log10(\bar{Y})$ values are greater and can be more easily seen compared to the $log10(mLCE)values$. We can compute both the mLCE and MEGNO of several random trajectories in the Henon-Heiles, 2D Standard Map and the 4D Standard map to study the global Dynamics of the system.

10.1 Global Dynamics of the Henon-Heiles System

The Global dynamics of the Henon-Heiles system is analysed by computing both MEGNO and mLE for 10 000 trajectories in the system as shown in Figure 16 and 17. Each trajectory is evolved over 3000 timesteps with $\tau = 0.1$. The initial (y, py) conditions of the trajectories are sampled randomly in the intervals $y \in [-0.3, 0.5]$, and $py \in [-0.2, 0.2]$. The initial px value are determined via equation 36.

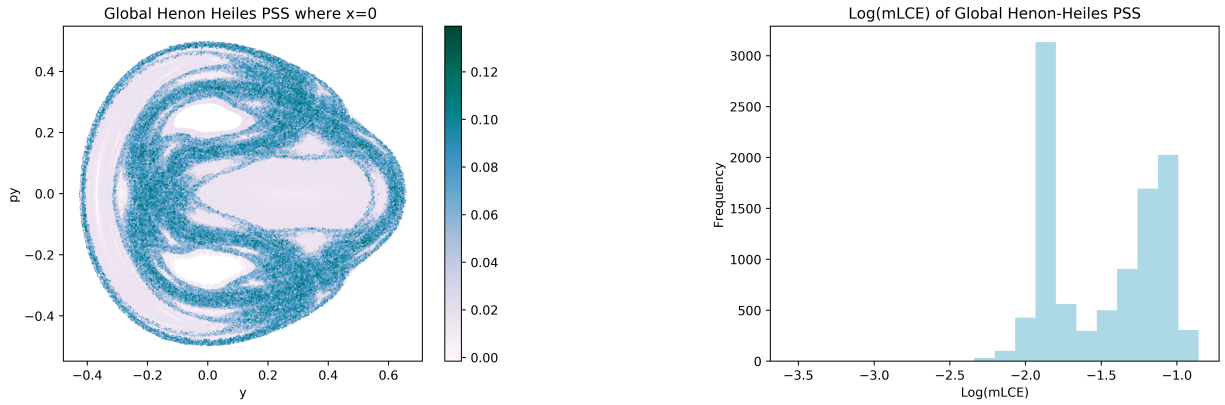

(a) Multiple Trajectories in the Henon-Heiles system

(b) Log10(mLCE) Indicator

Figure 16

The light pink areas in Figure 16a correspond to islands of stability with a small mLCE that is surrounded by blue regions of chaos. Figure 16a also shows the existence of cantori, the small stability regions around the larger stability islands(Dvorak,199). The colour of the points surrounding these regions are lighter than those found in the established chaotic regions which indicate a somewhat small mLCE. The darker pink points may reflect the presence of Sticky orbits that only grow (a small amount) after long time periods. Since Sticky orbits are Chaotic, the mLCE will likely misidentify these chaotic trajectories as regular.

Figure 16b shows the frequency of each log10(mLCE) value in the system. This figure shows that the the distribution of the log10(mLCE) values is binomial. The frequency of smaller log(mLCE) values reflect the amount of regular orbits there are in the system, whereas the number of larger log(mLCE) values reflect the amount of chaotic trajectories in the system. Determining at which mLCE value is a trajectory no longer considered regular since its' mLCE value is not close enough to 0 is a problem that will persists in all the systems studied in this report. A closer inspection of Figure 16 will reveal several light pink points in the chaotic regions. These points are clearly chaotic, however they correspond to a small mLCE value. The Frequency Histogram in figure (16b) that quantifies the number of chaotic and regular trajectories may therefore be inaccurate since it will incorrectly assume that chaotic trajectories are regular due to small mLCE values. If we consider any trajectories with $log10(mLCE) > -1.3$ values to be chaotic, then at least 60% of the trajectories of the system are chaotic.

Figure 17 similarly shows 10 000 random trajectories in Phase space as well as the MEGNO indicator for each of these trajectories. The colour of the trajectory reflects the final $\bar{Y}$ value of the trajectory. The PSS section in Figure 17a is similar to the one shown in figure 16. This is expected since MEGNO is a weighted variant of the mLCE and will thus behave similarly.

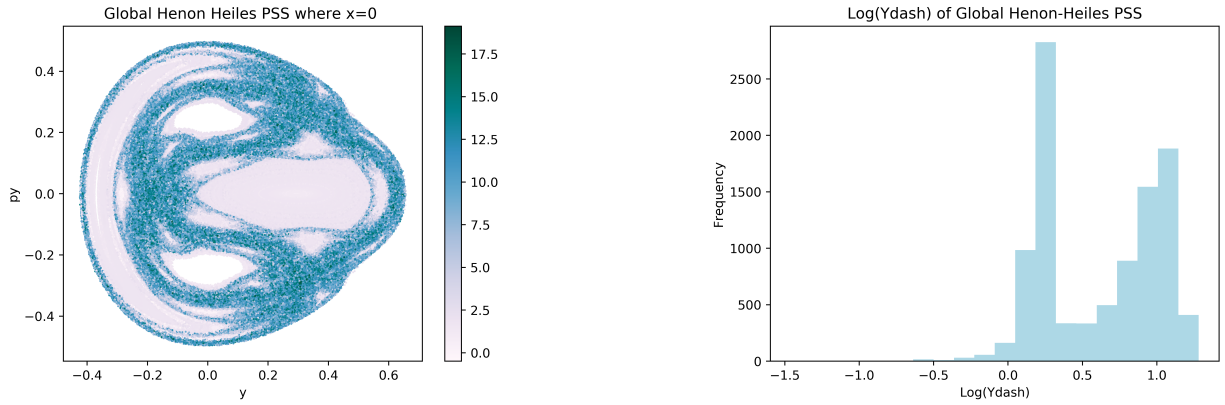

(a) Multiple Trajectories in the Henon-Heiles system

(b) Log10($\bar{Y}$) Indicator

Figure 17: Chaos indicators in Global dynamics of Henon-Heiles system

MEGNO provides a slightly better image that differentiates between regular and chaotic trajectories. The points in the chaotic region tend to be a darker colour which allows us to better differentiate chaotic and regular regions. Light pink points do still appear in the chaotic regions so some chaotic trajectories may be misclassified. However, since the colourbar reflects that trajectories with $5 > \bar{Y} > 2$ could still be light pink in the PSS, but classified as chaotic according to the MEGNO. Since MEGNO provides a criteria for chaos as shown in equation 42, it can be said that at least 3500 of the 10000 trajectories are classified as regular according to figure 17b. This means $\sim 65\%$ of the trajectories in Henon-Heiles system with $K = \frac{1}{8}$ is chaotic.

10.2 Global Dynamics of 2D Map

The chaos indicators can be used to study the global dynamics of Discrete systems. A simple discrete system is the 2D Standard Map. To begin, we take a random sample of 5000 initial points from ($x1 \in [0, 2\pi], x2 \in [0, 2\pi]$) and iterate them 2000 times. A Plot of these points as well as their corresponding mLCEs are shown in Figure 18.

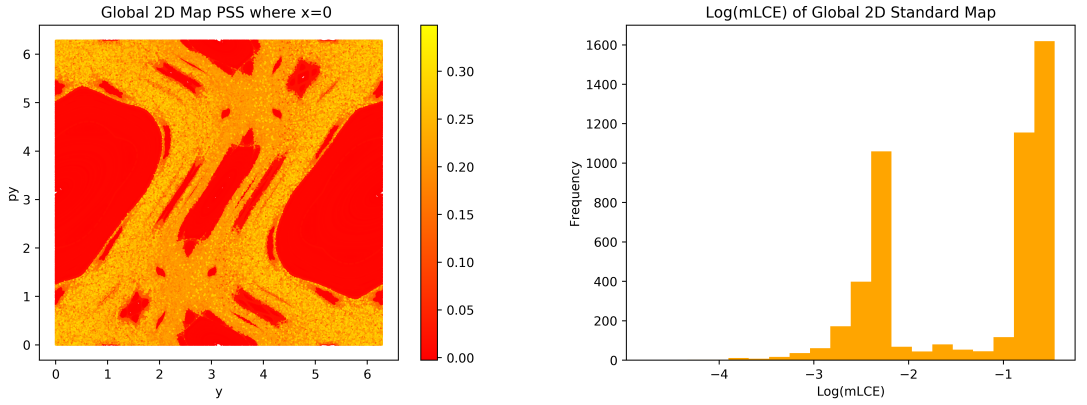

(a) Global Dynamics

(b) Analysing Global Dynamics using log10(mLCE)

Figure 18: Analysing the Global Dynamics of the 2D Map using mLCE

The red areas correspond to islands of stability in the system whereas the orange/ yellow region is the region of instability where chaotic and sticky orbits occur. The smaller red regions near the large islands of stability are the cantori that emerge when regular trajectories become chaotic.A closer inspection of figure **??** will reveal that orange points occur near the cantori that likely reflect sticky orbits with small mLCE values. These values are not small enough for us to classify these points as regular thus the mLCE can successfully classify sticky

orbits as chaotic.

The distribution of the log10(mLCE) values is similarly binomial compared to the log10(mLCE) values of the Henon-Heiles system. We will consider small log10(mLCE) values ($log10(mLCE) < -2$) to reflect regular trajectories. Red dots in figure 18a do appear in chaotic regions. The mLCE of these flows is small and will thus be incorrectly classified as regular according to the indicator.

The global dynamics of the 2D Map can be similarly analysed using MEGNO as shown in Figure 19. The plot of the points in figure 19a is similar to the plot in 18a. However, a close inspection of the centre island of stability in figure 19a shows that there exists some chaotic flows with $\bar{Y} >> 2$ that separate the islands into cantori near the edges of the island. The PSS in figure 19a also show red points in the regions of Chaos, however these values do not necessarily represent the $\bar{Y} = 2$ and do not reflect that MEGNO classifies these orbits as chaotic. This poses a problem as the Trajectories in the regular orbits can also have $\bar{Y} > 2$. This is a computational problem since the range of the $\bar{Y}$ values is larger than the range of values in the colour gradient.

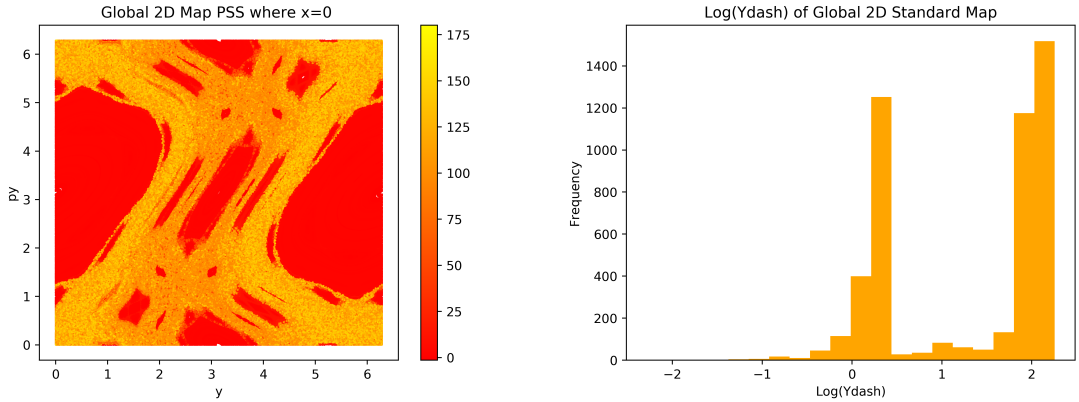

(a) Global Dynamics of 2D Map

(b) Analysing Global Dynamics using log10($\bar{Y}$)

Figure 19: Analysing the Global Dynamics of the 2D Map using MEGNO

The frequency histogram in figure 19b shows that at least ~ 2000 trajectories satisfies equation 42 and can be classified as regular out of the 10000 trajectories that were sampled. This shows that $\sim 80\%$ of the system is chaotic. We have now established how to using MEGNO and the mLCE to quantify the degree of chaos in a discrete system. We will now apply these methods to the more complex 4D Standard Map.

10.3 Global Dynamics of 4D Standard Map

The Global Dynamics of the 4D Standard Map can be analysed by evolving 50000 trajectories 5000 times and evaluating the mLCE and MEGNO for these trajectories. 4-dimensional Trajectories in the 4D Standard Map are difficult to visualise in 4D. We can reduce this by visualising the trajectories on a Poincare Surface section of the 4D Standard Map. The PSS is chosen where $x3 = 0, x4 = 0$ and the points $x1, x2$ are visualised.
We can begin studying the degree of chaos in the system by iterating 50000 initial points with $x4 = 0, x3 = 0$ and $x1, x2$ chosen randomly in the interval $[0, 1]$. If we set $x3, x4$ to 0, we have effectively kept the one of the two 2D maps constant while varying the other one. Once these points are finished iterating, we can compute a relatively accurate estimate of the mLCE of the trajectories that begins with these initial conditions. THe PSS of these flows as well as the frequency of each mLCE is shown in figure 20.

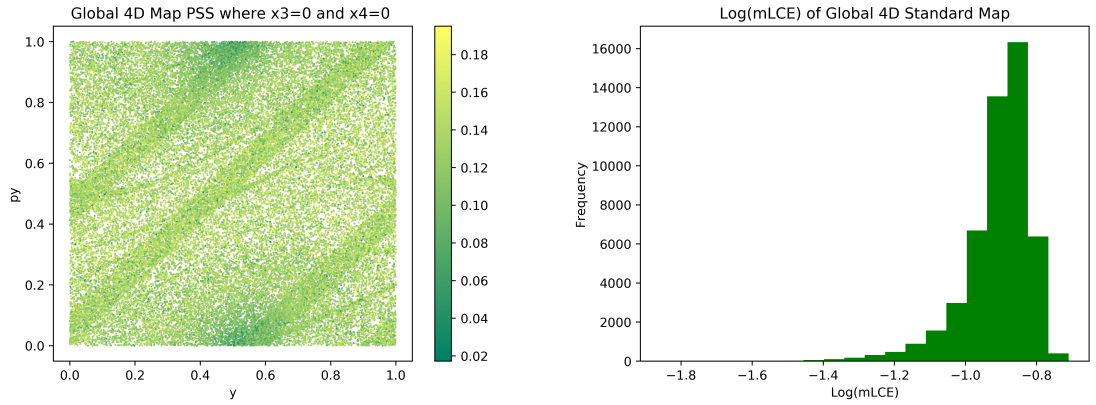

(a) Global Dynamics (b) Analysing Global Dynamics using log10(mLCE)

Figure 20: Analysing the Global Dynamics of the 4D Map using mLCE

Figure 20a shows that all the mLCE values in this system are relatively close together. There is therefore no means of discerning which trajectories are chaotic and which are regular. The mLCE in this context thus fails in quantifying the 'degree of chaos' in the 4D Standard Map. An attempt to use MEGNO to analyse the global dynamics of this system will similarly fail as shown in Figure 21.

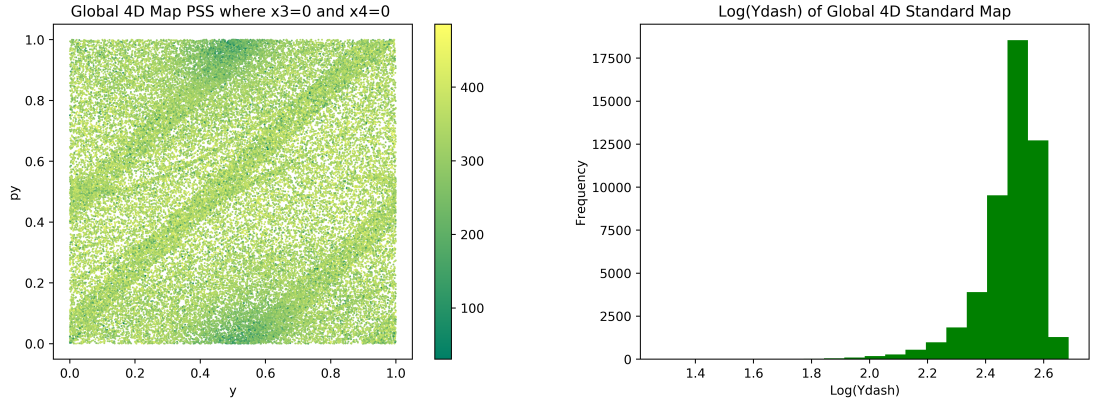

(a) Global Dynamics (b) Analysing Global Dynamics using log10(MEGNO)

Figure 21: Analysing the Global Dynamics of the 4D Map using mLCE

Although the PSS of the 4D map shown in Figure 20 and 21 fail to show where regions of chaos and stability occur, it does show sections that are dense with points. These are known as resonance islands. There are also signs of "chatter" where the resonant islands interact as there are thin structures that are beginning to emerge on the PSS (Moradi et al, 12). These structures indicate that the 4D Map may be a resonant system. These systems are characterized by resonance, when the natural frequencies of the system synchronise. Although these figures did not allow us to quantify the Degree of chaos in the system, it did give us more information about other aspects of the 4D Standard Map. If we change the variables that vary we may be able to find better chaos indicator values since the dynamics will differ greatly.

If we choose to keep $x2 = x4 = 0$ and vary $x1, x3$ instead, different dynamics will occur in the 4D Map. Since $x2 = 0$ now, we can choose a different PSS where $x2 = x4 = 0$. We will similarly randomly sample 10000 initial $x1, x3$ points from interval $[0, 1]$ and iterate them 2000 times. The number of initial points was reduced since iterating 50000 samples is time consuming and does not provide much better details on the system. Although the PSS surface will be sparse, it will still provide all the general details needed analyse the chaos dynamics of the system. The mLCE of 10000 random trajectories in shown in Figure 22.

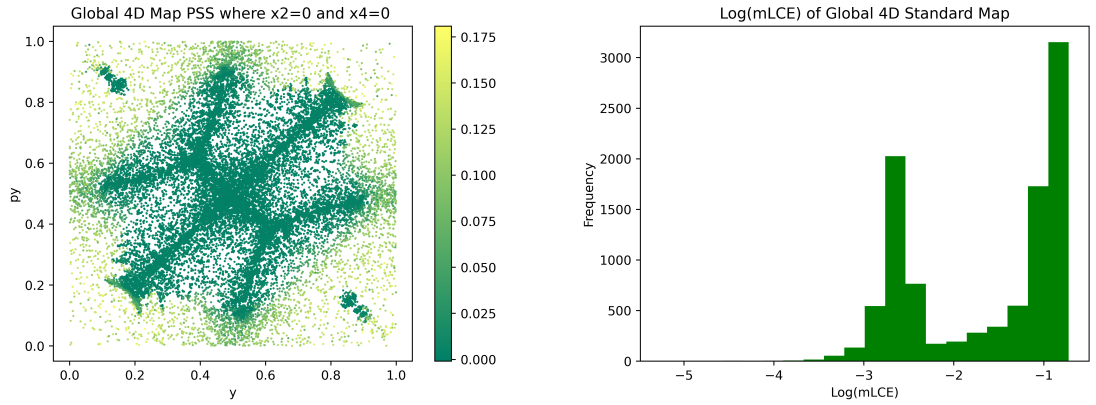

(a) Global Dynamics (b) Analysing Global Dynamics using log10(mLCE)

Figure 22: Analysing the Global Dynamics of the 4D Map using mLCE

The PSS shown above in Figure 22a is completely different to the one shown in Figure 20a. The mLCE values shown in figure 22b are also more consistent with the mLCE values found in the previous systems. Figure 22a shows that most of the regular trajectories occur in the centre of the PSS with chaotic trajectories emerging from the corners. A close look at the top left section of Figure 22a shows that there are still dark green dots with a small mLCE in that region of chaos. This shows that the mLCE will occasionally misidentify chaotic trajectories as regular, which is consistency with the findings of the previous two sections. The $log10(mLCE)$ values can be used to quantify the 'degree of chaos' in this particular system. If we take all trajectories with $log10(mLCE) < -2.5$ to be regular then $\sim 60\%$ of the trajectories are chaotic. We can similarly use MEGNO to infer the 'degree of chaos' in the system. Figure 23 shows the MEGNO indicator($\bar{Y}$) computed for 10000 random trajectories.

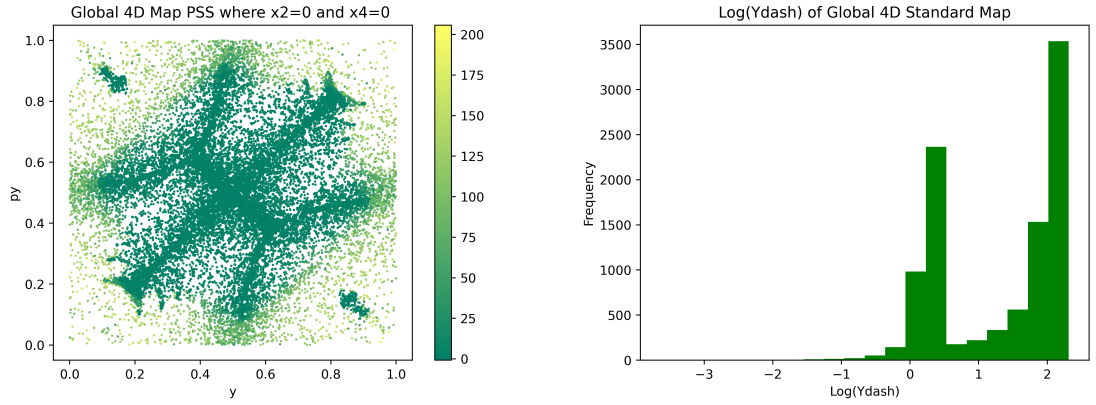

(a) Global Dynamics (b) Analysing Global Dynamics using log10(MEGNO)

Figure 23: Analysing the Global Dynamics of the 4D Map using mLCE

Figure 23 shows that the MEGNO indicator comes to the same conclusion as the mLCE; regular trajectories occur in the centre of the PSS in a 'X' shape with a line through it, whereas the chaotic regions occur in the corners of the Surface sections. The top left and bottom right corners in both PSS surface sections show two islands of stability. If we use the log10($\bar{Y}$) values in figure 23b as well as the criteria shown in equation 42, we will similarly conclude that the system has 60000 chaotic orbits out of 10000, or the degree of Chaos of the 4D Map when $x1, x3$ vary and $x2 = x4 = 0$ is $\sim 60\%$.

The 4D Standard map with the same K and B parameters will have different degrees of chaos, depending

on which variables are varies since changing the varying variable from $x3$ to $x2$ can shift the system from being $\sim 99\%$ chaotic to $\sim 60\%$ as shown above.

11 Conclusion

MEGNO is a variation of the mLCE that can better detect chaos compared to its predecessor (mLCE). It provides a clearer image on which orbits are chaotic and which are regular since the difference between Y values for chaotic and regular trajectories is large and grows over time. MEGNO also provides a solid criteria for trajectories to be considered regular. This criteria is also more easily satisfiable using numeric computation compared to the criteria for regular trajectories using the mLCE. The mLCE criteria also presents a difficulty in considering how small a value should be before it can be ≈ 0 and the corresponding trajectory regular. One potential weakness of MEGNO is that Y oscillates over time, however computing and using $\bar{Y}$ instead negates the oscillating problem. MEGNO and the mLCE can present unique problems depending on the specifics

MEGNO is a fast chaos indicator that can detect chaos efficiently in relatively short time periods. In the case of sticky orbits, MEGNO can classify it as chaotic before the 'sticky' behaviour even emerges. MEGNO can also be used to study the global dynamics of a system. Since all $\bar{Y} > 2$ will definitely be chaotic, it the ideal indicator to use when quantifying the degree of chaos in a system. Although MEGNO is slightly more difficult to compute compared to the mLCE, the benefits in efficiently and clarity outweigh this shortcoming of MEGNO. The mLCE is a fundamental chaos indicator with many modern variants that outperform it. We have shown that MEGNO is one of these variants by illustrating how MEGNO performs better at detecting chaos for a few (*Local*) trajectories as well as several (*Global*) trajectories.

12 References

References

[1] Benettin, G. et al. (1980) 'Lyapunov characteristic exponents for smooth dynamical systems and for Hamiltonian Systems; a method for computing all of them. part 1: Theory', Meccanica, 15(1), pp. 9–20. doi:10.1007/bf02128236.

[2] Calogero, F. (2011) 'Isochronous Dynamical Systems', Philosophical Transactions of the Royal Society A: Mathematical, Physical and Engineering Sciences, 369(1939), pp. 1118–1136. doi:10.1098/rsta.2010.0250.

[3] Contopolous, G. and Harsoula, M. (2008) 'Stickiness in chaos', International Journal of Bifurcation and Chaos, 18(10), pp. 2929–2949. doi:10.1142/s0218127408022172.

[4] Cincotta, P.M. and Giordano, C.M. (2016) 'Theory and applications of the mean exponential growth factor of nearby orbits (megno) method', Chaos Detection and Predictability, pp. 93–128. doi:10.1007/978-3-662-48410-4_4.

[5] Cline, D. and Sarkis, M. (2019) Variational principles in classical mechanics. Rochester, New York: University of Rochester River Campus Libraries.

[6] Devaney, R. (2021) Introduction to chaotic dynamical systems. S.l.: CRC PRESS.

[7] Dvorak, R. (1999) '"stickiness" in Dynamical Systems', The Dynamics of Small Bodies in the Solar System, pp. 509–534. doi:10.1007/978-94-015-9221-5_48.

[8] Henon, M. (1982) "On the numerical computation of Poincar e maps," Physica D: Nonlinear Phenomena, 5(2-3), pp. 412–414. Available at: https://doi.org/10.1016/0167-2789(82)90034-3.

[9] Laskar, J. and Robutel, P. (2001) "HIGH ORDER SYMPLECTIC INTEGRATORS FOR PERTURBED HAMILTONIAN SYSTEMS," Celestial Mechanics and Dynamical Astronomy, 80(1), pp. 39–62. Avail- able at: https://doi.org/10.1023/a:1012098603882

[10] Lichtenberg, A.J. and Lieberman, M.A. (1992) Regular and chaotic dynamics. New York City, New York State: Springer.

[11] Lega, E. and Froeschlé, C. (1997) 'Fast Lyapunov indicators comparison with other Chaos Indicators Application to two and four dimensional maps', The Dynamical Behaviour of our Planetary System, pp. 257–275. doi:10.1007/978-94-011-5510-6_18.

[12] Lega, E., Guzzo, M. and Froeschlé, C. (2016) 'Theory and applications of the fast lyapunov indicator (FLI) method', Chaos Detection and Predictability, pp. 35–54. doi:10.1007/978-3-662-48410-4_2.

[13] Maffione, N.P., Giordano, C.M. and Cincotta, P.M. (2011) 'Testing a fast dynamical indicator: The megno', International Journal of Non-Linear Mechanics, 46(1), pp. 23–34. doi:10.1016/j.ijnonlinmec.2010.06.008.

[14] Meiss, J.D. (2008) Symplectic maps. thesis.

[15] Mestre, M.F., Cincotta, P.M. and Giordano, C.M. (2011) 'Analytical relation between two chaos indicators: Fli and megno', Monthly Notices of the Royal Astronomical Society: Letters, 414(1). doi:10.1111/j.1745-3933.2011.01065.x.

[16] Moradi, H., Movahhedy, M.R. and Vossoughi, G. (2012) 'Dynamics of regenerative chatter and internal resonance in milling process with structural and cutting force nonlinearities', Journal of Sound and Vibration, 331(16), pp. 3844–3865. doi:10.1016/j.jsv.2012.03.003.

[17] Nunez, J.A., Cincotta, P.M. and Wachlin, F.C. (1996) 'Information entropy', CELESTIAL MECHANICS AND DYNAMICAL ASTRONOMY, 64(1–2), pp. 43–53. doi:10.1007/bf00051604.

[18] Satyal, S., Quarles, B. and Hinse, T.C. (2013) 'Application of chaos indicators in the study of dynamics of S-type extrasolar planets in stellar binaries', Monthly Notices of the Royal Astronomical Society, 433(3), pp. 2215–2225. doi:10.1093/mnras/stt888.

[19] Skokos, Ch. (2010) 'The Lyapunov characteristic exponents and their computation', Dynamics of Small Solar System Bodies and Exoplanets, pp. 63–135. doi:10.1007/978-3-642-04458-8_2.

[20] Strogatz, S. and Dichter, M. (2016) Nonlinear Dynamics and Chaos, second edition. Boulder: Westview Press.

[21] Tobin, R. (2009) "A Glance at the Standard Map." California: UCDavis

[22] Wells, S. (2022) Chaos theory explains why your life gets so unbelievably messy (and beautiful), Popular Mechanics. Available at: https://www.popularmechanics.com/science/a41334070/what-is-chaos-theory/ (Accessed: 22 May 2023).

[23] Wigmore, I. (2016) What is chaos theory?: Definition from TechTarget, WhatIs.com. Available at: https://www.techtarget.com/whatis/definition/chaos-theory (Accessed: 22 May 2023).

[24] Virtanen P et al. (2020) SciPy 1.0: Fundamental Algorithms for Scientific Computing in Python. Nature Methods, 17(3), 261-272.